Energy 148 (2018) 1060–1068

Contents lists available at ScienceDirect

Energy

journal homepage: www.elsevier.com/locate/energy

Direct contact membrane distillation system for waste heat recovery: Modelling and multi-objective optimization

Rui Long*, Xiaotian Lai, Zhichun Liu, Wei Liu**

School of Energy and Power Engineering, Huazhong University of Science and Technology, 1037 Luoyu Road, Wuhan 430074, China

ARTICLE INFO

Article history:
Received 30 October 2017
Received in revised form
18 January 2018
Accepted 8 February 2018
Available online 9 February 2018

Keywords:
Direct contact membrane distillation
Modelling
Heat recovery
Multi-objective optimization

ABSTRACT

Direct contact membrane distillation (DCMD) is an alternative technology to utilize the low temperature waste heat source for water supply. In this paper, we proposed a modified model characterizing the heat and mass transfer in the DCMD, which was validated by a great accordance with the experiment data. For evaluating the performance of a DCMD system with heat recovery, gain output ration (GOR) and mass recovery rate are two main criteria, however, they could not achieve their maximum values simultaneously. To achieve such a compromise, a multi-objective optimization considering both the water recovery rate and GOR was conducted. Besides, the GOR, mass recovery rate and thermal efficiency under single-objective optimization methods were calculated and compared. Compared to the results under the maximum GOR, the increase magnitude of water mass recovery rate under the multi-objective optimization override the decrease magnitude of GOR. Compared with the performance under the single-objective optimization for transmembrane water flux, the transmembrane water flux under the multi-objective optimization was reduced by only 6.7%, but the GOR is increased by 83.2%.

1. Introduction

Membrane distillation (MD) is of practical application for everyday life and industry utilization, such as sea water distillation, fruit processing and waste water treatment [1]. The reality of the MD process mainly relies on the hydrophobic membrane that allows the water vapor pierce through, and serves as a barrier for the liquid phase. There are many kinds of MD configurations, such as direct contact membrane distillation (DCMD), air-gap membrane distillation (AGMD), sweeping-gas membrane distillation (SGMD), and vacuum membrane distillation (VMD) [2]. Among them, DCMD is the most extensively investigated due to its relative simplicity on the system scale for industrial application. In the DCMD system, a porous hydrophobic membrane is installed to separate the feed liquid stream and the permeate liquid stream. And the operating temperature and pressure are much lower [3]. Therefore, DCMD can also be used to recovery waste heat and utilize the low grade renewable thermal energy for water supply, thus to alleviate the fast depletion of fossil fuels [4–6]. The vapor permeates through the membrane due to the difference of the partial vapor pressure at the membrane-liquid interface, induced by the temperature difference of the feed and permeate solutions. The evaporation and condensation take place in the solid matrix of the hydrophobic membrane. There is no obvious phase transition, thus the operation of the DCMD system is of much less demand.

Key parameters impacting the performance of the DCMD process are membrane properties as well as operating conditions and module specifications. In the DCMD process, the heat and mass transfer happen across the hydrophobic membrane simultaneously. The mass transfer is solely induced by the partial vapor pressure difference beside the two sides of the membrane. However, there are mainly two ways for heat transfer from the high temperature feed solution to the low temperature permeate solution: convective heat transfer carried by the transmembrane water flux and heat conduction through the porous hydrophobic membrane. Therefore, the membrane properties play a very important role on the performance of the DCMD process. The overall performance of the membrane should be of high mass transfer coefficient and low heat conductivity. Phattaranawik et al. [7] investigated the influence of pore size distribution and air fluxes on water vapor fluxes across the membranes, and found that the transition region was the major contribution to mass transport. Li et al. [8] studied the membrane properties on the performance of the DCMD performance. Janajreh et al. [9] researched the DCMD performance under different configurations, velocities and membrane properties based on a 2D heat transfer model.

* Corresponding author.
** Corresponding author.
E-mail addresses: r_long@hust.edu.cn (R. Long), w_liu@hust.edu.cn (W. Liu).

https://doi.org/10.1016/j.energy.2018.02.027
0360-5442/

To study the performance of the DCMD system, experimental investigation plays an important role. Yun et al. [3] carried an experiment study on the performance of the DCMD process with high concentration NaCl aqueous solutions, and found that water fluxes decrease with increasing concentration of NaCl solutions and more sharply at higher concentrations. Hwang et al. [10] applied a commercially available polytetrafluoroethylene membrane in DCMD to experimentally investigate the module dimension effect on performance. As experimental study could not cover all the operating situations of the DCMD system, simulations offer an effective way to study and predict the performance of the DCMD system more directly [11]. Qtaishat et al. [12] developed a mathematical model to describe the mass and heat transfer in the DCMD by considering the feed thermal boundary layer. Manawi et al. [13] presented a model by taking into account the varying operating conditions to predict the flux and temperature polarization along the membrane. Chen et al. [14] developed a two-dimensional mathematical model to predict the temperature polarization profile of the DCMD process. Swaminathan et al. [15] developed a membrane distillation model based on heat exchanger theory for different kinds of membrane distillation technologies. Yang et al. [16] studied the heat and mass transfer processes in DCMD under laminar flow conditions through a 2D heat transfer model by computational fluid dynamics (CFD). Hitsov et al. [17] presented a one-dimension model for the simulation of the flux and energy efficiency of a full-scale DCMD module, which considered the membrane compaction effects. Bui et al. [18] presented a new procedure for modelling the simultaneous heat and mass transfer in DCMD in a hollow fiber configuration based on semi-empirical models, employing the analogy between heat and mass transfer, which considered the effect of fiber length and tortuosity in the bundle and fiber size. Karam et al. [19] presented a lumped-parameter dynamic model for the DCMD system to study the performance under wide range of steady-state and dynamic conditions.

Main performance specifications for the DCMD system are the water productivity, and energy efficiency. Much efforts have been devoted to improve the performance of the DCMD process. Ho et al. [20] used roughened-surface flow channel to enhance the countercurrent-flow DCMD system and around 42.11% of the performance enhancement was obtained. Yang et al. [21] explored micro-structured hollow fiber designs with wavy-and gear-shaped cross sections to enhance the DCMD performance to depolarize the buildup of liquid boundary layers, thus increasing water productivity. Yang et al. [22] employed turbulence promoters in the hollow fiber MD to improve the performance of the MD process. And the optimal transmembrane mass flux is improved by 74%. Yu et al. [23] investigated the heat mass transfer improvement by applying annular baffles to the hollow fiber modules, and found that baffles could greatly enhance the mass flux when the heat-transfer resistance is mainly dominated in the liquid boundary layers. Yang et al. [24] applied the Janus hollow fiber membrane with a mussel-inspired coating on the lumen surface to improve the performance of the DCMD system, and the water flux is improved by 120%. Besides the improvement of the membrane properties and module channel structure, further revision of the pure DCMD system can also significantly enhance the overall performance. Duong et al. [25] experimentally studied the DCMD system with brine recycling and found that brine recycling could increase water recovery and thermal efficiency. Furthermore, DCMD with heat regeneration (DCMD-RE) is also investigated to enhance the energy efficiency [26]. In addition, other performance criteria are also investigated. Deshpande et al. [27] conducted a systematic numerical analysis focusing on exergy destruction inside the module, and investigated the operational and geometric parameters to maximize recovery ratio with constraints on exergetic efficiency.

DCMD with heat regeneration is one of most feasible improvements of the DCMD system. Much efforts have been focused on the performance optimization of the DCMD system with heat recovery [26]. The system energy efficiency is defined as gain output ratio (GOR). However, based on the Aspen Plus software, Guan et al. [28] studied the performance of the DCMD system with heat recovery, and found the contradictory relationship of the GOR and the water productivity. Furthermore, although the CFD simulation could describe the DCMD process more deeply, it is not applicable for design and system optimization considering its huge computing duration. Therefore, the one-dimension model based on mass and heat conservation is still appealing due to its relatively less computing time required. In previous studies on describing the mass and heat transfer processes based on the one-dimension model, either the mass and heat transfer coefficients are treated as constants during the modeling process to simplify the differential governing equations, or based on the electrical analogy, the average temperature during the heat transfer process is adopted to calculate the average heat and mass transfer coefficients, thus to obtain the performance specifications of the DCMD system. Actually, they could not fulfill the real situations satisfactorily. In present study, we are focused on the performance of a DCMD with regeneration (DCMD-RE) system. As the system consists of two components, there exist coupling of thermal energy transfer between the singular DCMD system and the regenerator. If we both choose the experimental expressions to describe the DCMD-RE system, the results obtained maybe deviate significantly from the real ones. Therefore, we describe the heat and mass transfer processes in the DCMD and regenerators based on the differential equations with heat and mass balances. In addition, the heat and mass transfer coefficients are modeled as temperature depended parameters based on previous studies. In this sense, our revised model could demonstrate the heat and mass transfer processes more close to the real ones of the DCMD-RE systems. In order to take into account the effect of temperature on the mass transfer coefficient and flow regimes, a revision one-dimension model base on Ref. [26] is presented to analyze the DCMD system with heat regeneration.

Furthermore, the mass recovery rate is widely adopted to evaluate the performance of the DCMD systems. However the GOR for a singular DCMD system is rather low, resulting in the birth of the DCMD-RE system to increase the GOR. In real life, we both want the mass recovery rate and GOR are as high as possible. However, previous and present studies have revealed that the mass recovery rate and the GOR could not achieve their maximum values simultaneously. To coordinate the GOR and water recovery rate of the system, the NSGA-II is employed to obtain the Pareto frontier with maximum water recovery rate and COR as the objective functions. As the Pareto set reflects different weights of the two objectives, the TOPSIS is applied to identify the final optimal point of the studied system. The GOR, water recovery rate, and thermal efficiency of the DCMD with recovery under the optimal conditions are obtained. For comparison, the performance under the corresponding single-objective optimization is also investigated. The temperature and concentration profiles under different optimization methods are systematically analyzed. Then the performance under the multi-objective optimization with different feed solution temperature and concentrations are also presented. Finally, some remarking conclusions are drawn.

2. Model development

The water distillation system for waste heat recovery is illustrated in Fig .1. High concentration feed solution absorbs heat from the low grade waste heat, then evaporates in the DCMD process,

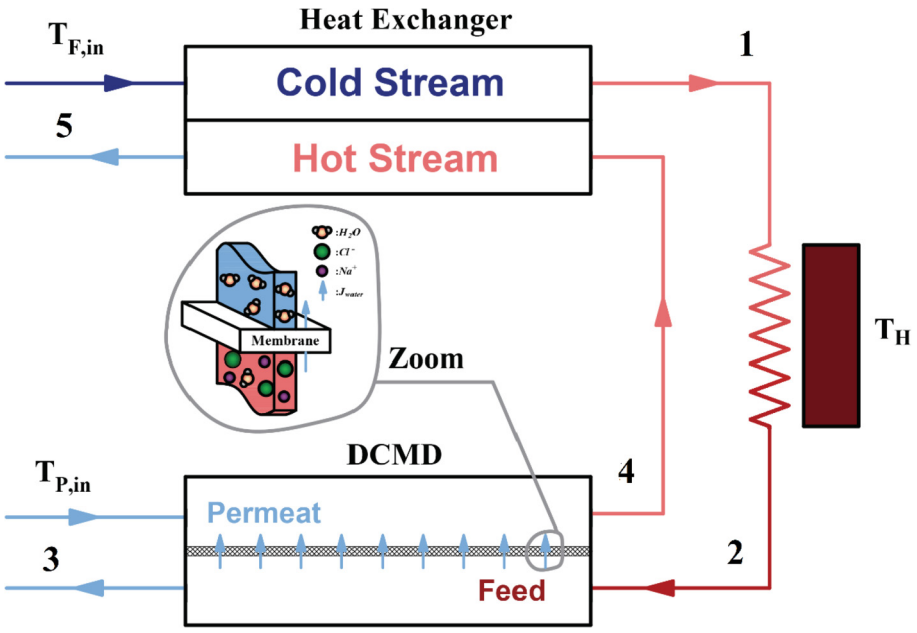

Fig. 1. Schematic diagram of counter flow DCMD-RE system.

meanwhile the permeate solution remains at a relatively lower temperature. Driven by the partial water vapor pressure difference aside the membrane, transmembrane water pierces across the membrane. To improve the system performance, a regenerator (RE) is employed to decrease the heat absorbed from the heat source, thus to augment the system energy efficiency.

2.1. DCMD heat and mass transfer characteristics

In the DCMD process, the mass transport is usually described by assuming a linear relationship between the mass flux and the water vapor pressure difference [29]

$$J_w = B_m(p_F - p_P) \tag{1}$$

where B_m is the mass transfer coefficient, determined by membrane properties and operating conditions; p_F and p_P are the partial water pressures on the vapor–liquid interfaces at the feed and permeate sides.

The water vapor pressure (p^v) at given temperature T is [30]

$$p^v = \exp\left(23.1964 - \frac{3816.44}{T - 46.13}\right) \tag{2}$$

The partial vapor pressure at the membrane surface in the feed solution with molar fraction of salt f can be calculated as [31]

$$p_F = (1 - f)\left(1 - 0.5f - 10f^2\right)p^v \tag{3}$$

To determine the mass transfer coefficient, the flow patterns in the porous membrane must be considered, which can be classified into the Knudsen region, ordinary diffusion region and transition region, depending on the Knudsen number. For most of the cases, the flow pattern lies in the transition region with the mass transfer coefficient given by

$$B_m = 1\Big/\left(1\Big/B^D + 1\Big/B^K\right) \tag{4}$$

where B^K and B^D are, respectively the mass transfer coefficient in the Knudsen region ($K_n > 1$) and ordinary diffusion region ($K_n < 0.01$).

$$B^K = \frac{2}{3}\frac{\varepsilon r}{\tau\delta}\left(\frac{8M}{\pi RT}\right)^{1/2} \tag{5}$$

$$B^D = \frac{\varepsilon}{\tau\delta}\frac{PD}{P_a}\frac{M}{RT} \tag{6}$$

where ε, τ, r, and δ are the porosity, tortuosity, pore radius and membrane thickness, respectively; P is the total pressure inside the pore, and D is the water diffusion coefficient.

Based on the mass conservation, we have governing equations at any position x in the feed and permeate channels:

$$\frac{dm_F(x)}{dx} = \frac{A_{MD}}{L_{MD}}B_m(x)\left(p_f(x) - p_p(x)\right) \tag{7}$$

$$\frac{dm_P(x)}{dx} = \frac{A_{MD}}{L_{MD}}B_m(x)\left(p_f(x) - p_p(x)\right) \tag{8}$$

Along with the mass transfer across the hydrophobic membrane, heat is transferred from the high temperature feed solution to low temperature permeate solution via the transmembrane water as well as conduction through the solid matrix of the membrane. According to Ref. [26], the energy conservation of the feed solution and the permeate reads:

$$\frac{d[m_F(x)h_L(C(x),T_F(x))]}{dx} = \frac{dm_F(x)}{dx}\left[h_{vap}(C(x),T_F(x)) + h_L(0,T_F(x))\right] + \frac{A_{MD}}{L_{MD}}\xi_F(x) \tag{9}$$

$$\frac{d[m_P(x)h_L(0,T_P(x))]}{dx} = \frac{dm_P(x)}{dx}\left[h_{vap}(0,T_P(x)) + h_L(0,T_P(x)) + c_{p,V}(T_F(x) - T_P(x))\right] + \frac{A_{MD}}{L_{MD}}\xi_P(x) \tag{10}$$

where $\xi_F(x)$ and $\xi_P(x)$ are the conductive heat transfer at the permeate-membrane/ feed-membrane interface, which are, respectively, deduced as [26]:

$$\xi_F(x) = \frac{J_w C_{p,v}}{\exp(C_{p,v}\delta J_w/k_{MD}) - 1}(T_F - T_P) \tag{11}$$

$$\xi_P(x) = \frac{J_w C_{p,v}\exp(C_{p,v}\delta_m J_w/k_{MD})}{\exp(C_{p,v}\delta J_w/k_{MD}) - 1}(T_F - T_P) \tag{12}$$

where $k_{MD} = \varepsilon k_v + (1-\varepsilon)k_s$ is the overall heat conductive coefficient with k_v and k_s being the heat conductive coefficient for water vapor and solid matrix, respectively. $C_{p,v}$ is the heat capacity of the water vapor.

Based on Equations (7)-(10), we can calculate the temperature and mass flow rate distribution along the process direction with the boundary conditions given by:

$$T_F(L_{MD}) = T_2, \quad T_P(0) = T_{P,in} \tag{13}$$

$$m_F(L_{MD}) = m_{F,in}, \quad m_F(0) = \alpha m_{F,in} \tag{14}$$

where α is the relative flow rate of the permeate solution and the feed solution. For given temperature and concentration of the salt solution, the relative flow rate is the main parameter affecting the performance of the DCMD system.

2.2. Heat transfer in the regenerator

In order to enhance the efficiency of the DCMD system, a regenerator is applied to utilize the thermal energy of the permeate solution to preheat the feed solution. Given the energy conservation, the governing equations for the heat transfer characteristic in the regenerator are written as [26,32]

$$m_h \frac{dh_L(0, T_h(x))}{dx} = K_{RE}\frac{A_{RE}}{L_{RE}}[T_h(x) - T_c(x)] \tag{15}$$

$$m_c \frac{dh_L(C_1, T_c(x))}{dx} = K_{RE}\frac{A_{RE}}{L_{RE}}[T_h(x) - T_c(x)] \tag{16}$$

where K_{RE} is the heat transfer coefficient of the regenerator with A_{RE} and L_{RE} being the heat transfer area and length, respectively. T_h indicates the temperature for the hot stream, and T_c for the cold stream. The temperature profiles along the regenerator can be calculated by solving the energy balance equations (16) and (17), with the boundary conditions listed below:

$$T_h(L_{RE}) = T_4, \quad T_c(0) = T_{F,in} \tag{17}$$

2.3. Performance specifications of the DCMD-RE system

To evaluate the performance of the DCMD-RE system, there are two main criteria: gain output ratio (GOR) and mass recovery rate. GOR reflects the energy efficiency of the system driven by the external heat source, mass recovery rate indicates how much the transmembrane water can be produced.

The GOR is defined as

$$GOR = \frac{\int_0^{L_{MD}} J_w \Delta h dx}{Q_H} \tag{18}$$

where Δh is the evaporation enthalpy. Heat Q_H absorbed from the low temperature waste heat source is given by

$$Q_H = m_{F,in}(h_1 - h_2) \tag{19}$$

The mass recovery rate ξ can be defined as the ratio between the *trans*-membrane flow rate and the influent feed flow rate:

$$\xi = \Delta m_{MD}/m_{F,in} \tag{20}$$

In addition, thermal efficiency of the singular DCMD process, evaluating the performance of the DCMD process itself is given by

$$\eta = \frac{\int_0^{L_{MD}} J_w \Delta h dx}{Q_{MD}} = \frac{\int_0^{L_{MD}} J_w \Delta h dx}{m_{F,in}h_2 - m_{F,out}h_3} \tag{21}$$

where h_3 is the outlet enthalpy of the feed solution in the DCMD process.

3. Impacts of relative flow rate on the system performance

3.1. Model validation

The model presented in this paper is validated by the measured data from Ref. [10]. The DCMD module is of 0.5 m length and 0.15 m width. Under different inlet velocities of the salt solution, the outlet temperatures of the feed and permeate solutions and the transmembrane water flux are calculated. In the calculation, the NaCl concentration of the feed solution is 1%wt. The inlet temperature is 333.15 K for the feed solution, and 293.15 K for the permeate solution. The model studied in this paper can be justified by the good accordance between the results calculated and experimental measured data as show in Fig. 2.

3.2. Sensitivity analysis

To give a first impression of the behavior with the different relative flow rate of the permeate and feed solutions in a DCMD-RE system, the model is used to simulate the DCMD system equipped with the hydrophobic membrane as adopted in Ref. [10]. The DCMD module is of 2 m length and the active area of the membrane is 16 m^2. The membrane porosity is 0.83, and tortuosity is 2.52. The thermal conductivity is 0.12 $W/(m^2 \cdot K)$. The active area of the regenerator is 24 m^2 with 4 m length. The heat transfer coefficient is preset as 1000 $W/(m^2 \cdot K)$. Fig. 3 shows the relation of GOR, thermal efficiency, and mass recovery rate of the relative flow rate. The GOR first increases with increasing relative flow rate of the permeate and feed solutions, reaches its maximum value, then decreases. Thermal efficiency also presents the same tendency with increasing relative flow rate. But it decreases rather slowly after achieving its maximum value. The optimal value corresponding to the maximum GOR does not coincide with that leading to the maximum value of the thermal efficiency. The relative flow rate corresponding to the maximum thermal efficiency is less than that leading to the maximum GOR. The GOR indicates the degree of the external heat utilized, which includes the energy efficiency of the DCMD-RE system, while the thermal efficiency only presents the performance of the membrane distillation. It can be seen that heat regeneration can significantly augment the performance of the membrane distillation. The mass recovery rate first increases with increasing relative flow rate, reaches its maximum value, then stays constant. There exists a minimally relative flow rate leading to the maximum value of the mass recovery rate.

4. Performance optimization

Multi-objective optimization is widely adopted to coordinate the conflicting performance specifications, whose results are usually a set of non-dominated solutions (Pareto frontier) with

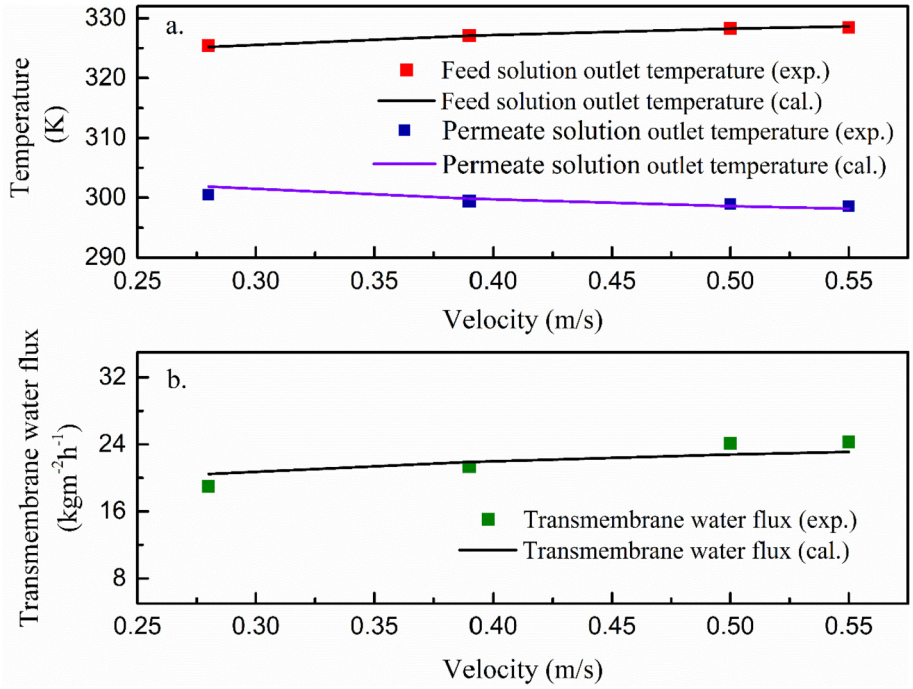

Fig. 2. Validation of the model. Calculated (line) and measured (square points) outlet temperature and transmembrane water flux as a function of the volume flow rate. The NaCl concentration is 1%wt. The inlet temperature is 333.15 K for the feed solution, and 293.15 K for the permeate solution.

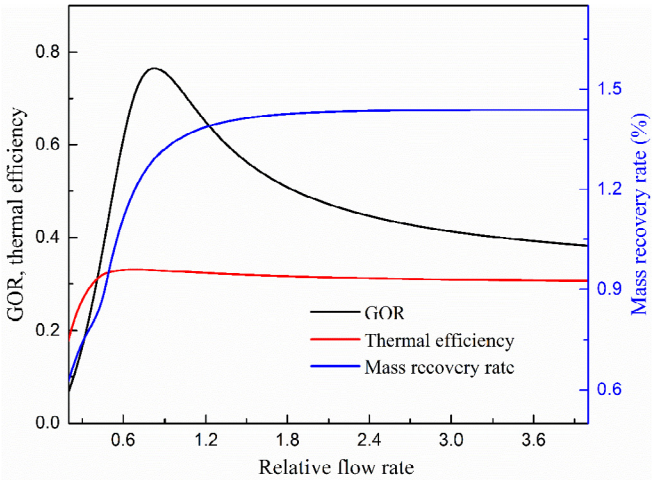

Fig. 3. GOR, thermal efficiency, and mass recovery rate as a function of the relative flow rate. The inlet temperature is 323.15 K for the feed solution, and 293.15 K for the permeate solution.

minimum conflict between the objectives. As each point in the Pareto frontier represents certain weights of the objectives, to select the final optimal point, decision-making techniques should be employed, such as LINMAP, TOPSIS, and Belman–Zadeh methods [33,34], among which the TOPSIS has been widely applied, indicating the maximum deviation from the non-ideal point and a minimum deviation from the ideal point.

To evaluate the performance of the above system, the GOR and mass recovery rate are both two important performance specifications. The GOR reflects the utilization degree of the low temperature waste heat. And the mass recovery rate manifests how much we can get. As mentioned above, the optimal relative flow rate leading to the maximum value of the GOR does not agree with that corresponding to the maximum mass recovery rate. They could not achieve their maximum value simultaneously. In order to coordinate the performance of the DCMD system, an optimization based on NSGA-II has been conducted to achieve an appropriate compromise between the GOR and the mass recovery rate.

4.1. Pareto frontier and the final optimal point

Fig. 4 depicts the Pareto frontier calculated through the multi-objective optimization for the DCMD system with different concentrations, which illustrates the obvious repugnant phenomenon

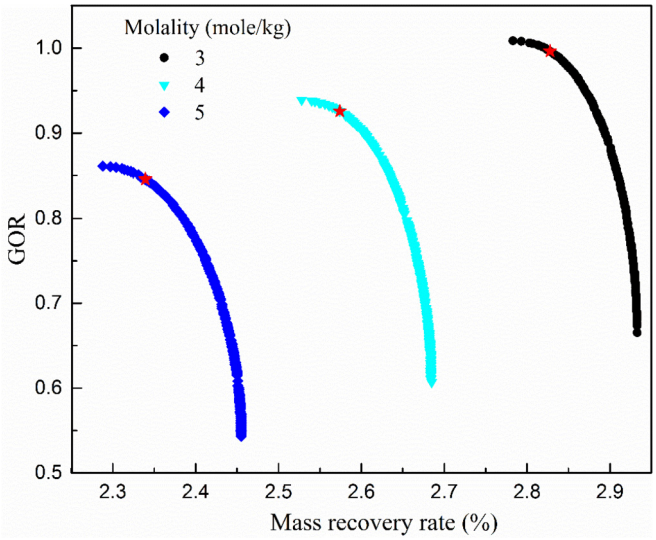

Fig. 4. Pareto frontier from multi-objective optimization of the DCMD system with heat recovery under different molalities. The star-marked points are obtained by the TOPSIS algorithm. The inlet temperature is 343.15 K for the feed solution, and 293.15 K for the permeate solution.

of the maximum GOR and transmembrane water flux. As each point in the Pareto frontier represents certain weights of the two conflicting objectives, the top-left point represents the GOR is mostly weighted, corresponding to the single objective optimization for GOR, whereas the bottom-right indicates the transmembrane water flux is mostly weighted, in accord with the situation under the single objective optimization for transmembrane water flux. The Pareto frontier shifts left with increasing concentration of the feed solution. What's more, the larger concentration, the lower maximum value of the GOR and transmembrane water flux. The star-marked points represent the final optimal point selected by the TOPSIS algorithm. For a prescribed concentration of the feed solution, under the multi-objective optimization, the GOR and water recovery rate exhibit moderate values, as shown in Fig. 4.

4.2. Performance comparison between different optimization methods

To start with, the temperature profiles along the normalized axis poison in the MD and the regenerator under different optimization methods are depicted in Fig. 5. These temperatures present different characteristics under different relative flow rates. The permeate solution absorbs heat from the feed solution in the MD module, then heat up the feed solution in the regenerator. Previous literature about the MD with regenerator illustrates that for given concentration of the feed solution, the performance of the MD are dominated by the relative flow rate. Based on the relative magnitude of the relative flow rate, the operating specification can be classified into three operating regions, i.e. the permit limiting regime (PLR), feed limiting regime (FLR) and mass transfer limited regime (MTLR) [26]. In the PLR, the relative flow rate is small, thus the permeate solution is insufficient. In the FLR, the feed solution is insufficient. The driving force of MD process vanishes, and the feed solution drops from T_H to T_C*, where T_C* can be calculated by solving the equation $p_w(0, T_C) = p_w(C_F, T_C^*)$, which is shown in Fig. 5 under the optimization for transmembrane water flux. When the *trans*-membrane coefficient or the hydrophobic membrane area is not larger enough, the temperature of the permeate solution could not increase to T_H*, and that of the feed solution could not drop to T_C*. This is the MTLR as shown in Fig. 5 under the optimization for GOR and under the multi-objective optimization. Furthermore, as illustrated in Fig. 5, the insufficient permeate or feed solution in the FLR leads to limited heat transfer in the regenerator (RE), and the MTLR results in unlimited heat transfer in the RE.

Under different optimization methods, the mass flow rates of the permeate and feed solutions along the MD process are depicted in Fig. 6. Along the axial position, the mass flow rate of the permeate solution increases, while that of the feed solution decreases, as water vapor pierces through the hydrophobic membrane from the feed solution into the permeate solution driven by the pressure difference. The optimal mass flow rate of the permeate flow under the single-objective optimization for transmembrane water flux is the largest, and that under the single-objective optimization for GOR is the smallest. Under the optimization for maximum transmembrane water flux, the optimal relative mass flow rate takes the maximum value in the optimization space, which is much larger than those obtained under the other two optimization methods. Due to the process characteristics of the DCMD, the concentration of the feed solution is the highest under the maximum optimization for transmembrane water flux, and that under the optimization for GOR is the lowest, as shown in Fig. 7. As multi-objective optimization presents a compromise between the above two objectives, the outlet concentration and mass flow rates exhibit moderate values.

The GOR, thermal efficiency and transmembrane water flux under different optimization methods are depicted in Fig. 8. Compared with the performance under the single-objective optimization for GOR, the GOR under the multi-objective optimization was reduced by only 1.8%, but the transmembrane water flux is increased by 2.4%. Compared with the performance under the single-objective optimization for transmembrane water flux, the transmembrane water flux under the multi-objective optimization was reduced by only 6.7%, but the GOR is increased by 83.2%. What's more, thermal efficiencies under different optimization methods are also shown in Fig. 8. The thermal efficiency under the multi-objective optimization presents a moderate value.

4.3. Performance under different feed solution temperatures

For further investigating the performance of the DCMD system under the multi-objective optimization. The performance

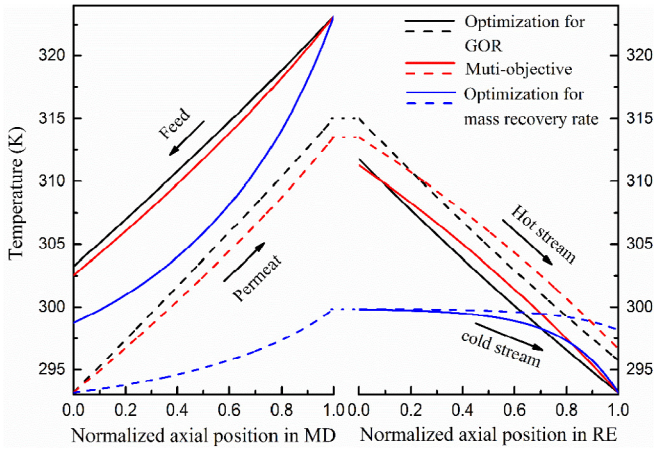

Fig. 5. Temperature profiles of the permeate and feed solutions in the MD, regenerator (RE) under different optimization methods. At the outlet of the MD, the permeate solution flows into the regenerator to heat up the cold stream. Hence the temperature of the permeate effluent is equivalent to that of the hot stream in the regenerator, which is denoted by the dot connecting lines. In the calculations, the inlet temperature is 323.15 K for the feed solution, and 293.15 K for the permeate solution.

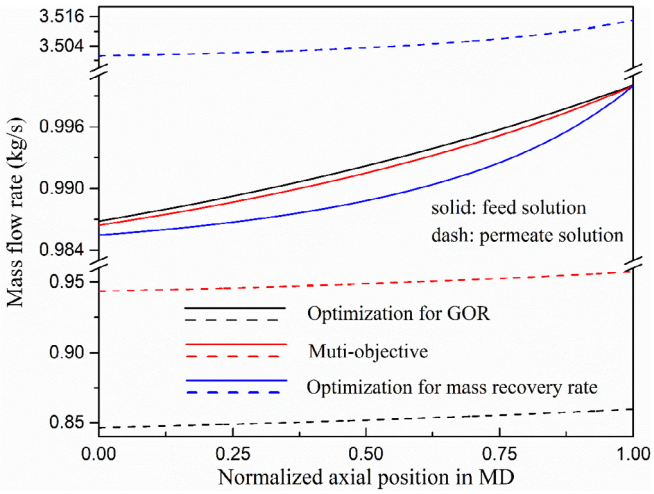

Fig. 6. Profiles for mass flow rate of the permeate and feed solutions in the MD under different optimization methods. In the calculations, the inlet temperature of the permeate solution is fixed at 20 °C and the inlet temperature of the feed solution is 50 °C.

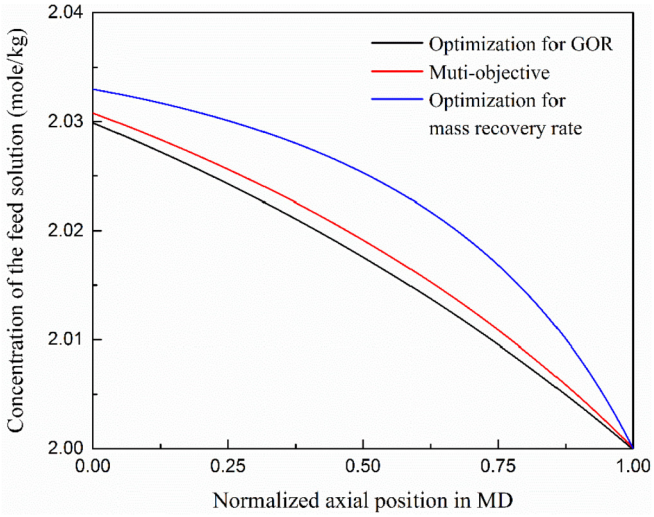

Fig. 7. Concentration profile for the feed solutions in the MD under different optimization methods. In the calculations, the inlet temperature of the permeate solution is fixed at 20 °C and the inlet temperature of the feed solution is 50 °C.

specifications under different inlet temperature of the feed solution and the corresponding optimal relative flow rate of the permeate and feed solutions are presented in Fig. 9. Fig. 9(a) shows the relation between the GOR and the feed solution inlet temperature under the multi-objective optimization. The GOR under the optimal condition nearly increases linearly with increasing inlet temperature of the feed solution. The lower molality of the feed solution, the larger the GOR. The mass recovery rate increases with increasing inlet temperature of the feed solution, but it increases more rapidly at higher temperatures, as shown in Fig. 9(b). The thermal efficiency also increases with increasing feed solution temperature. Unlike the trend of the mass flow rate with increasing temperature of the feed solution, it increases rather slowly at higher temperatures. In addition, the larger molality of the feed solution, the lower mass flow rate and thermal efficiency of the DCMD system, as depicted in Fig. 9(b) and (c). Furthermore, the optimal relative flow rate decreases with increasing heat source temperature. At higher temperatures, Larger MD feed NaCl concentration leads to lower optimal relative flow rate, while at lower temperatures, lower MD feed NaCl concentration results in lower optimal relative flow rate due to the coupling effects of the heat transfer properties and vapor pressure difference attached to the hydrophobic membrane, which are shown in Fig. 9(d).

5. Conclusions

As to the DCMD system, the water separation degree as water recovery rate and the energy efficiency (such as thermal efficiency for singular DCMD system and GOR for the DCMD-RE system) are main parameters characterizing the system performance. The qualified membrane distillation system should be of high water recovery rate and energy efficiency to meet the actual demand. The DCMD-RE system is one of the most feasible improvement for the singular DCMD system. Practically, the water recovery rate and GOR could not achieve their maximum value simultaneously. The study of the compromise between the above two criteria helps to designing and operating actual DCMD-RE systems.

In this paper, a refined model based on previous literature is developed to simulate the process of the DCMD-RE system by take into account the temperature depended mass and heat transfer characteristics. This model is validated by great agreement with the experiment data. For given feed solution temperature and concentration, the performance is determined by the relative mass flow rate between the permeate and the feed solution. There exists an optimal relative mass flow rate leading to the maximum GOR, while the mass recovery rate reaches a plateau at higher relative flow rates where the GOR decreases. To achieve a compromise between the maximum value of the mass flow rate and GOR, an optimization based on NSGA-II was conducted to obtain the Pareto

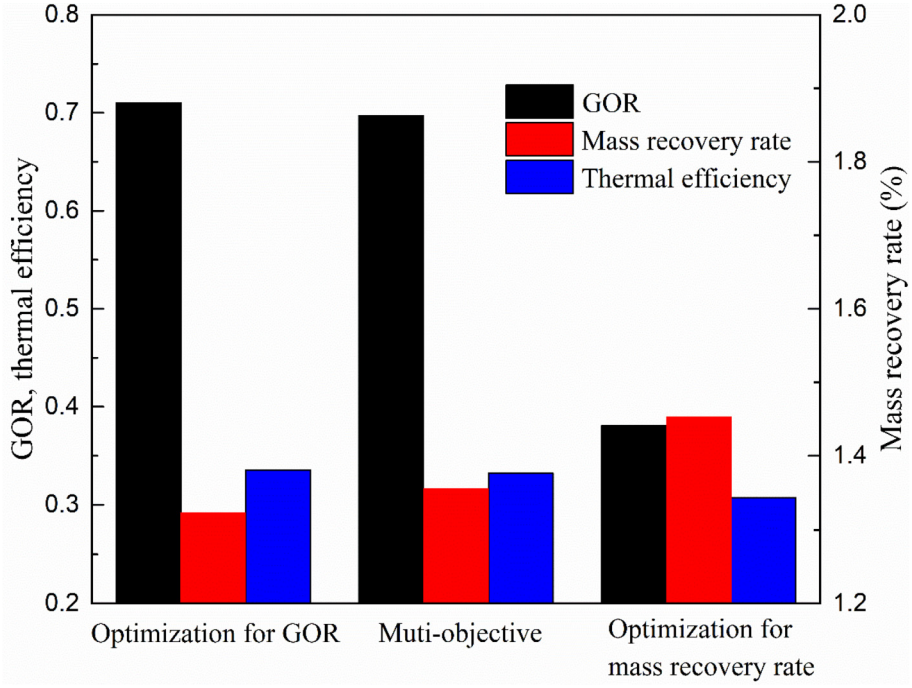

Fig. 8. Comparison of GOR, thermal efficiency and transmembrane water flux under different optimization objectives. In the calculations, the inlet temperature of the permeate solution is fixed at 20 °C and the inlet temperature of the feed solution is 50 °C.

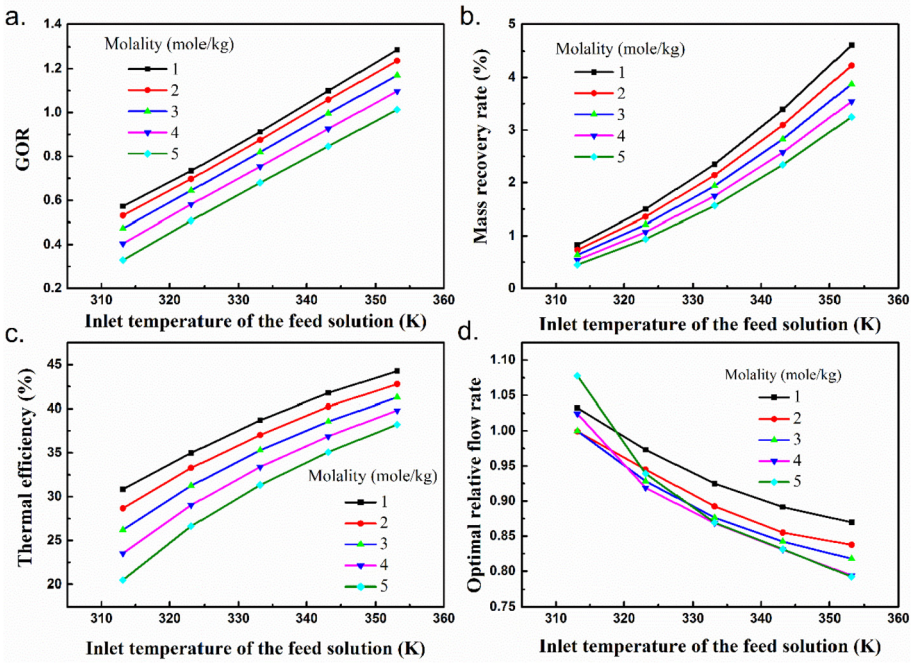

Fig. 9. GOR (a), mass recovery rate (b), thermal efficiency (c) Optimal relative MD permeate/feed solution flow rate (d) of the DCMD system as a function of feed solution inlet temperature under the multi-objective optimization with NaCl molarities varing from 1.0 mol/kg to 5.0 mol/kg in DCMD feed solution. In the calculations, the inlet temperature of the permeate solution is fixed at 293.15 K.

frontiers of the DCMD-RE system with different feed solution temperature and concentration. And the TOPSIS decision-making method was used to choose the final optimum design point of the system. In order to further investigate the system performance under multi-objective optimization, the performance specifications under the corresponding single-objective optimization methods were calculated and compared. For a prescribed feed solution temperature of 323.15 K and concentration of 2 mol/kg, compared with the performance under the single-objective optimization for GOR, the GOR under the multi-objective optimization was reduced by only 1.8%, but the transmembrane water flux is increased by 2.4%. Compared with the performance under the single-objective optimization for transmembrane water flux, the transmembrane water flux under the multi-objective optimization was reduced by only 6.7%, but the GOR is increased by 83.2%. Under different optimization methods, the thermal efficiencies do not present obvious difference. The operation parameters obtained by the multi-objective optimization can well balance both the mass recovery rate and GOR, thus to serve as a guidance for designing and running actual DCMD-RE system.

Acknowledgments

We acknowledge the support received from the National Natural Science Foundation of China (51706076, 51736004).

Nomenclature

A_{RE}	Heat transfer area m^2
B_m	Mass transfer coefficient $kg/(m^2 \cdot s \cdot K)$
B^K	Mass transfer coefficient in the Knudsen region $kg/(m^2 \cdot s \cdot K)$
B^D	Mass transfer coefficient in the ordinary diffusion region $kg/(m^2 \cdot s \cdot K)$
C_F	Concentration of feed solution mole/kg
$C_{p,v}$	Heat capacity of the water vapor kJ/(kg·K)
D	Water diffusion coefficient m^2/s
h	Enthalpy kJ/kg
J_w	Water flux m/s
K_{RE}	Heat transfer coefficient of the regenerator $w/(m^2 \cdot K)$
k_{MD}	Overall heat conductive coefficient w/(m·K)
k_v	Heat conductive coefficient for water vapor w/(m·K)
k_s	Heat conductive coefficient for solid matrix w/(m·K)
L_{RE}	Heat transfer length m
P	Total pressure inside the pore MPa
p_F	Partial water pressure at the feed side MPa
p_P	Partial water pressure at the permeate side MPa
p^v	Water vapor pressure MPa
Q_H	Heat absorbed from the low temperature waste heat source kW
r	Pore radius m
T	Temperature K
x	Molar fraction of salt
Δh	Evaporation enthalpy kJ/kg

Greek symbols

α	Relative flow rate of the permeate solution and the feed solution
ε	Porosity
τ	Tortuosity
δ	Membrane thickness m
ξ	Mass recovery rate
η	Efficiency

Superscript

v	Vapor
Kn	Knudsen region
D	Ordinary diffusion region

Subscripts

F	Feed solution
P	Permeate solution

h	Hot stream
c	Cold stream
v	Vapor
1–5	States in the system

Abbreviations

DCMD	Direct contact membrane distillation
GOR	Gain output ration
MD	Membrane distillation
AGMD	Air-gap membrane distillation
SGMD	Sweeping-gas membrane distillation
VMD	Vacuum membrane distillation
CFD	Computational fluid dynamics
RE	Regenerator
PLR	Permit limiting regime
FLR	Feed limiting regime
MTLR	Mass transfer limited regime

References

[1] Baghbanzadeh M, Rana D, Lan CQ, Matsuura T. Zero thermal input membrane distillation, a zero-waste and sustainable solution for freshwater shortage. Appl Energy 2017;187:910–28.

[2] Tang N, Zhang H, Wang W. Computational fluid dynamics numerical simulation of vacuum membrane distillation for aqueous NaCl solution. Desalination 2011;274(1):120–9.

[3] Yun Y, Ma R, Zhang W, Fane AG, Li J. Direct contact membrane distillation mechanism for high concentration NaCl solutions. Desalination 2006;188(1):251–62.

[4] Bouguecha ST, Boubakri A, Aly SE, Al-Beirutty MH, Hamdi MM. Solar driven DCMD: performance evaluation and thermal energy efficiency. Chem Eng Res Des 2015;100:331–40.

[5] Long R, Bao YJ, Huang XM, Liu W. Exergy analysis and working fluid selection of organic Rankine cycle for low grade waste heat recovery. Energy 2014;73(0):475–83.

[6] Suárez F, Ruskowitz JA, Tyler SW, Childress AE. Renewable water: direct contact membrane distillation coupled with solar ponds. Appl Energy 2015;158:532–9.

[7] Phattaranawik J, Jiraratananon R, Fane AG. Effect of pore size distribution and air flux on mass transport in direct contact membrane distillation. J Membr Sci 2003;215(1):75–85.

[8] Li L, Sirkar KK. Influence of microporous membrane properties on the desalination performance in direct contact membrane distillation. J Membr Sci 2016;513:280–93.

[9] Janajreh I, Suwwan D, Hashaikeh R. Assessment of direct contact membrane distillation under different configurations, velocities and membrane properties. Appl Energy 2017;185(Part 2):2058–73.

[10] Hwang HJ, He K, Gray S, Zhang J, Moon IS. Direct contact membrane distillation (DCMD): experimental study on the commercial PTFE membrane and modeling. J Membr Sci 2011;371(1–2):90–8.

[11] Chang H, Hsu JA, Chang CL, Ho CD, Cheng TW. Simulation study of transfer characteristics for spacer-filled membrane distillation desalination modules. Appl Energy 2017;185:2045–57.

[12] Qtaishat M, Matsuura T, Kruczek B, Khayet M. Heat and mass transfer analysis in direct contact membrane distillation. Desalination 2008;219(1–3):272–92.

[13] Manawi YM, Khraisheh M, Fard AK, Benyahia F, Adham S. Effect of operational parameters on distillate flux in direct contact membrane distillation (DCMD): comparison between experimental and model predicted performance. Desalination 2014;336(1):110–20.

[14] Chen TC, Ho CD, Yeh HM. Theoretical modeling and experimental analysis of direct contact membrane distillation. J Membr Sci 2009;330(1–2):279–87.

[15] Swaminathan J, Chung HW, Warsinger DM, Lienhard VJH. Membrane distillation model based on heat exchanger theory and configuration comparison. Appl Energy 2016;184:491–505.

[16] Yu H, Yang X, Wang R, Fane AG. Numerical simulation of heat and mass transfer in direct membrane distillation in a hollow fiber module with laminar flow. J Membr Sci 2011;384(s 1–2):107–16.

[17] Hitsov I, Eykens L, Schepper WD, Sitter KD, Dotremont C, Nopens I. Full-scale direct contact membrane distillation (DCMD) model including membrane compaction effects. J Membr Sci 2017;524:245–56.

[18] Bui VA, Vu LTT, Nguyen MH. Modelling the simultaneous heat and mass transfer of direct contact membrane distillation in hollow fibre modules. J Membr Sci 2010;353(1–2):85–93.

[19] Karam AM, Alsaadi AS, Ghaffour N, Laleg-Kirati TM. Analysis of direct contact membrane distillation based on a lumped-parameter dynamic predictive model. Desalination 2017;402:50–61.

[20] Ho CD, Huang CH, Tsai FC, Chen WT. Performance improvement on distillate flux of countercurrent-flow direct contact membrane distillation systems. Desalination 2014;338(1):26–32.

[21] Yang X, Yu H, Wang R, Fane AG. Optimization of microstructured hollow fiber design for membrane distillation applications using CFD modeling. J Membr Sci 2012;421–422(3):258–70. s.

[22] Yang X, Yu H, Wang R, Fane AG. Analysis of the effect of turbulence promoters in hollow fiber membrane distillation modules by computational fluid dynamic (CFD) simulations. J Membr Sci 2012;415–416(10):758–69. s.

[23] Yu H, Yang X, Wang R, Fane AG. Analysis of heat and mass transfer by CFD for performance enhancement in direct contact membrane distillation. J Membr Sci 2012;405–406(s 405–406):38–47. s.

[24] Yang H-C, Zhong W, Hou J, Chen V, Xu Z-K. Janus hollow fiber membrane with a mussel-inspired coating on the lumen surface for direct contact membrane distillation. J Membr Sci 2017;523:1–7.

[25] Duong HC, Cooper P, Nelemans B, Cath TY, Long DN. Optimising thermal efficiency of direct contact membrane distillation by brine recycling for small-scale seawater desalination. Desalination 2015;374:1–9.

[26] Lin S, Yip NY, Elimelech M. Direct contact membrane distillation with heat recovery: thermodynamic insights from module scale modeling. J Membr Sci 2014;453:498–515.

[27] Deshpande J, Nithyanandam K, Pitchumani R. Analysis and design of direct contact membrane distillation. J Membr Sci 2017;523:301–16.

[28] Guan G, Yang X, Wang R, Fane AG. Evaluation of heat utilization in membrane distillation desalination system integrated with heat recovery. Desalination 2015;366:80–93.

[29] Schofield RW, Fane AG, Fell CJD. Heat and mass transfer in membrane distillation. J Membr Sci 1987;33(3):299–313.

[30] Fernández-Pineda C, Izquierdo-Gil MA, Garcıa-Payo MC. Gas permeation and direct contact membrane distillation experiments and their analysis using different models. J Membr Sci 2002;198(1):33–49.

[31] Lawson KW, Lloyd DR. Membrane distillation. J Membr Sci 1997;124(1):1–25.

[32] Long R, Li B, Liu Z, Liu W. Hybrid membrane distillation-reverse electrodialysis electricity generation system to harvest low-grade thermal energy. J Membr Sci 2017;525:107–15.

[33] Long R, Li B, Liu Z, Liu W. Multi-objective optimization of a continuous thermally regenerative electrochemical cycle for waste heat recovery. Energy 2015;93(Part 1):1022–9.

[34] Ahmadi P, Rosen MA, Dincer I. Multi-objective exergy-based optimization of a polygeneration energy system using an evolutionary algorithm. Energy 2012;46(1):21–31.